

# Dual-wavelength mode-locked quantum-dot laser, via ground and excited state transitions: experimental and theoretical investigation

Maria Ana Cataluna,<sup>1,\*</sup> Daniil I. Nikitichev,<sup>1</sup> Spiros Mikroulis,<sup>2</sup> Hercules Simos,<sup>2</sup>  
Christos Simos,<sup>2</sup> Charis Mesaritakis,<sup>2</sup> Dimitris Syvridis,<sup>2</sup> Igor Krestnikov,<sup>3</sup>  
Daniil Livshits,<sup>3</sup> and Edik U. Rafailov<sup>1</sup>

<sup>1</sup> University of Dundee, School of Engineering, Physics and Mathematics, Dundee, DD1 4HN, UK

<sup>2</sup> University of Athens, Department of Informatics and Telecommunications Panepistimiopolis Ilisia, Athens, Greece

<sup>3</sup> Innolume GmbH, Konrad-Adenauer-Allee 11, Dortmund, Germany

\*m.a.cataluna@dundee.ac.uk

**Abstract:** We report a dual-wavelength passive mode locking regime where picosecond pulses are generated from both ground ( $\lambda = 1263\text{nm}$ ) and excited state transitions ( $\lambda = 1180\text{nm}$ ), in a GaAs-based monolithic two-section quantum-dot laser. Moreover, these results are reproduced by numerical simulations which provide a better insight on the dual-wavelength mode-locked operation.

©2010 Optical Society of America

**OCIS codes:** (140.4050) Mode-locked lasers; (140.5960) Semiconductor lasers; (250.5590) Quantum-well, -wire and -dot devices; (320.7120) Ultrafast phenomena.

---

## References and links

1. E. U. Rafailov, M. A. Cataluna, and W. Sibbett, "Mode-locked quantum-dot lasers," *Nat. Photonics* **1**(7), 395–401 (2007).
2. A. Markus, J. X. Chen, C. Paranthoen, A. Fiore, C. Platz, and O. Gauthier-Lafaye, "Simultaneous two-state lasing in quantum-dot lasers," *Appl. Phys. Lett.* **82**(12), 1818–1820 (2003).
3. M. A. Cataluna, E. U. Rafailov, A. D. McRobbie, W. Sibbett, D. A. Livshits, and A. R. Kovsh, "Ground and excited-state modelocking in a two-section quantum-dot laser," in *18th Annual Meeting of the IEEE Lasers and Electro-Optics Society, LEOS 2005*, Tech. Dig. LEOS 2005), 870–871.
4. M. A. Cataluna, W. Sibbett, D. A. Livshits, J. Weimert, A. R. Kovsh, and E. U. Rafailov, "Stable mode locking via ground- or excited-state transitions in a two-section quantum-dot laser," *Appl. Phys. Lett.* **89**(8), 081124 (2006).
5. J. R. Liu, Z. G. Lu, S. Raymond, P. J. Poole, P. J. Barrios, and D. Poitras, "Dual-wavelength 92.5 GHz self-mode-locked InP-based quantum dot laser," *Opt. Lett.* **33**(15), 1702–1704 (2008).
6. A. Leitenstorfer, C. Fürst, and A. Laubereau, "Widely tunable two-color mode-locked Ti:sapphire laser with pulse jitter of less than 2 fs," *Opt. Lett.* **20**(8), 916–918 (1995).
7. C. W. Luo, Y. Q. Yang, I. T. Mak, Y. H. Chang, K. H. Wu, and T. Kobayashi, "A widely tunable dual-wavelength CW Ti:sapphire laser with collinear output," *Opt. Express* **16**(5), 3305–3309 (2008).
8. C. Song, W. Xu, Z. Luo, A. Luo, and W. Chen, "Switchable and tunable dual-wavelength ultrashort pulse generation in a passively mode-locked erbium-doped fiber ring laser," *Opt. Commun.* **282**(22), 4408–4412 (2009).
9. H. Yoshioka, S. Nakamura, T. Ogawa, and S. Wada, "Dual-wavelength mode-locked Yb:YAG ceramic laser in single cavity," *Opt. Express* **18**(2), 1479–1486 (2010).
10. J. Kim, M.-T. Choi, and P. J. Delfyett, "Pulse generation and compression via ground and excited states from a grating coupled passively mode-locked quantum dot two-section diode laser," *Appl. Phys. Lett.* **89**(26), 261106 (2006).
11. E. A. Viktorov, P. Mandel, A. G. Vladimirov, and U. Bandelow, "Model for mode locking in quantum dot lasers," *Appl. Phys. Lett.* **88**(20), 201102 (2006).
12. M. Sugawara, N. Hatori, H. Ebe, M. Ishida, Y. Arakawa, T. Akiyama, K. Otsubo, and Y. Nakata, "Modelling room-temperature lasing spectra of 1.3 self-assembled InAs/GaAs quantum-dot lasers: Homogeneous broadening of optical gain under current injection," *J. Appl. Phys.* **97**(4), 043523 (2005).
13. M. Sugawara, T. Akiyama, N. Hatori, Y. Nakata, H. Ebe, and H. Ishikawa, "Quantum-dot semiconductor optical amplifiers for high-bit-rate signal processing up to 160 Gb/s<sup>-1</sup> and a new scheme of 3R regenerators," *Meas. Sci. Technol.* **13**(11), 1683–1691 (2002).
14. D. B. Malins, A. Gomez-Iglesias, S. J. White, W. Sibbett, A. Miller, and E. U. Rafailov, "Ultrafast electroabsorption dynamics in an InAs quantum dot saturable absorber at 1.3  $\mu\text{m}$ ," *Appl. Phys. Lett.* **89**(17), 171111 (2006).

## 1. Introduction

In recent years, mode-locked quantum-dot (QD) lasers have shown great promise as compact ultrashort-pulse laser sources [1], due the useful combination of ultrafast absorption recovery with the possibility of broad gain/absorption bandwidth and low threshold current values. Furthermore, QD materials exhibit a set of discrete energy levels, and as such laser emission can occur via ground-state (GS), excited-state (ES) or via both GS and ES transitions simultaneously [2]. Exploiting this potential in ultrashort-pulse generation, we have previously reported the first demonstration of mode-locking via ground or excited state transitions in a quantum-dot laser [3,4]. Nevertheless, the GS mode-locking regime did not coexist with the ES regime, and it was necessary to change the bias conditions (gain current and absorber reverse bias) in order to switch between one mode-locking regime and the other. More recently, dual-wavelength mode-locking was reported for a single-section InP-based QD laser diode, with pulses being generated simultaneously at 1543 and 1571nm [5]. However, these spectral bands are not ascribed to the ES/GS transitions – the authors point out the hypothesis that the energy-level splitting corresponds to the Rabi oscillation frequency. Furthermore, due to the absence of a saturable absorber section or external mode-locking stimulus, the mechanism for the pulse generation in this single-section laser is not yet fully understood.

Dual-wavelength mode-locked laser sources have been traditionally developed and investigated with other solid-state materials, most notably in Ti:Sapphire [6,7], fiber [8] and most recently, ceramic lasers [9]. Research in this area has been motivated by the variety of applications for dual- and multiple-wavelength ultrashort pulses, such as time-domain spectroscopy, nonlinear optical frequency conversion and wavelength division multiplexing. In this context, the compactness, lower cost and direct electrical pumping associated with semiconductor lasers are very attractive features for reducing the footprint and complexity of the aforementioned applications, with the potential to also open up new avenues in ultrafast optical processing and optical interconnects.

In this paper, we report a dual-wavelength passive mode-locking regime where pulses are generated from both GS ( $\lambda = 1263\text{nm}$ ) and ES ( $\lambda = 1180\text{nm}$ ) transitions, from a two-section QD laser diode - the widest spectral separation (83nm) ever observed in a dual-wavelength mode-locked non-vibronic laser [6]. We also present numerical simulations obtained by means of a theoretical model based on the delay differential equation approximation, which are in good qualitative agreement with the above behavior.

## 2. Device structure and experimental setup

The QD structure used in the laser device was grown by molecular beam epitaxy on a GaAs substrate. The active region incorporated 5 layers of InAs QDs. A two-section QD laser diode was fabricated with a ridge waveguide  $6\mu\text{m}$  wide, a total length of 2mm, while the saturable absorber was  $300\mu\text{m}$  long, and was located near the back facet. The front and back facets were anti-reflection ( $\sim 3\%$ ) and high-reflection ( $\sim 95\%$ ) coated, respectively.

The laser was operated at room temperature ( $20^\circ\text{C}$ ), with its temperature thermoelectrically controlled via a Peltier cooler. The gain section was pumped with a low-noise current source and the absorber section was connected to a voltage source. The threshold current increased between 48mA and 180mA for reverse bias voltage values between 2V and 10V, while the slope efficiency decreased from 0.35mW/mA to 0.24mW/mA for the same voltage range. The pulse durations in both GS and ES spectral bands were measured by a non-collinear autocorrelator based on second-harmonic generation. The spectral characteristics were measured by a spectrometer and mode-locking performance was further investigated with an RF spectrum analyzer in combination with a high-speed 29GHz photodiode.

### 3. Experimental results and discussion

The dual-wavelength mode locking regime was obtained for current levels in the gain section between 330 and 430mA, and values of reverse bias between 6 and 10V in the saturable absorber section. A map depicting the different mode-locking regimes is represented in Fig. 1. It is noteworthy to point out that mode-locking involving solely the ES transition is observed both before and after the dual-wavelength mode-locking regime.

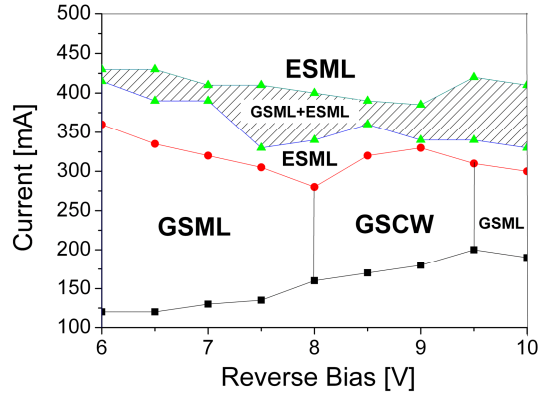


Fig. 1. Mapping of the different operating regimes observed in this laser. The dashed region corresponds to the dual-wavelength mode-locking regime here described (GSML + ESML). Legend: GSML – ground-state mode-locking; ESML – excited-state mode-locking; GSCW – ground-state continuous wave operation.

The central emission wavelengths were 1180nm and 1263nm for ES and GS, respectively [Fig. 2(a)]. Due to the different refractive index for the two wavelengths, this spectral separation was translated into a difference in pulse repetition rates for ES and GS, which were 19.6GHz and 20.1GHz respectively [Fig. 2(b)].

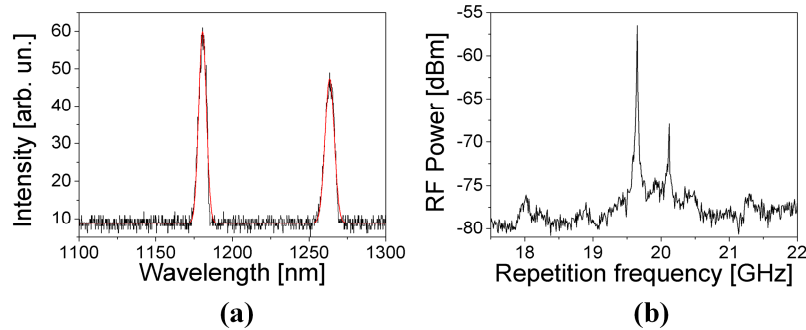


Fig. 2. (a) Optical spectrum and (b) RF spectrum characteristic of the dual-wavelength mode-locked regime, for a reverse bias of 6V and an injection current of 425mA (the red line in a) depicts the Gaussian fit to the ES and GS spectral bands). In the RF spectrum, the observed power difference between GS and ES is a result of the different optical power level and pulse duration for each of the pulse trains, as elucidated in the text.

In Fig. 3, the autocorrelation traces obtained for the ES and GS are shown, evidencing pulse durations of 8.6ps for the ES and 5.9ps for the GS bands, obtained for a reverse bias of 6V and an injection current of 425mA. The pulses were both highly chirped, exhibiting time-bandwidth products (TBWP) of 6.7 for the GS and 9 for the ES. These pulse durations and TBWPs are similar to those previously observed in separate GS/ES mode-locking [4,10].

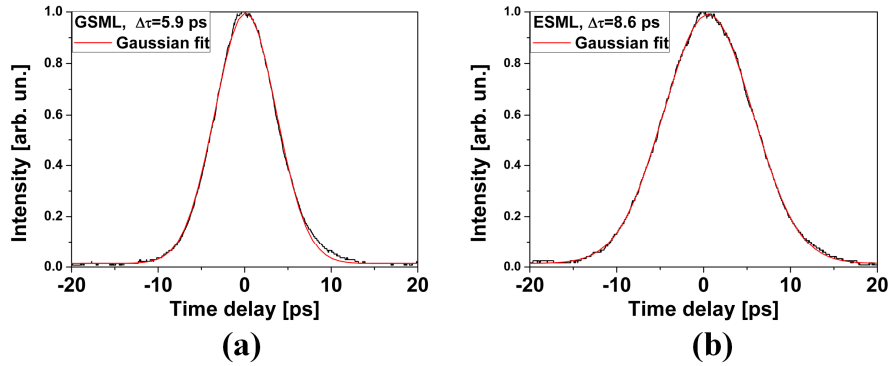


Fig. 3. Autocorrelation traces for (a) pulses generated via GS mode-locking; (b) pulses generated via ES mode-locking (for a reverse bias of 6V and an injection current of 425mA).

It is important to stress that, although not equal, the average power was of the same order for GS and ES (in the range of  $\sim 20$ - $30$  mW), which we believe to be an important factor in achieving a stable pulsed operation for both, owing to the dynamics of absorption saturation in a passively mode-locked laser. For instance, under the bias conditions examined in Figs. 2 and 3, the average power for the GS was  $P_{GS} = 21.3$  mW and for the ES was  $P_{ES} = 32.1$  mW. The difference of  $\sim 10$  dB between the GS and ES peaks, as shown in the RF spectrum [Fig. 2(b)], can be accounted for as follows. According to the Fourier analysis properties of a Gaussian pulse train, the amplitude of its Fourier transform depends on both the power of the pulse, as well as its duration - the broader the pulse, the higher the RF peak. The power ratio between ES and GS corresponds to  $P_{ES}/P_{GS} = 1.5$ , while the pulses generated via the ES are broader by a factor of 1.46 than the GS pulses, for the same conditions. As such, the amplitude of the Fourier transform for the ES will be  $\sim 2.2$  times higher ( $\sim 3.5$  dB difference) than that corresponding to the GS, which can justify a difference of approximately  $\sim 7$  dB (the double) in the electrical power spectrum. Importantly, a difference of  $\sim 8$  dB is also obtained from the numerical simulations as depicted in Fig. 5(b) on the next section, corresponding to the pulses represented in Fig. 5(a) (in the figure, the pulses are shown normalized). The remaining difference between the experimental observation ( $\sim 10$  dB) and the above calculations ( $\sim 7$  dB), can be due to experimental conditions, such as variations in the average power, the RF spectrum analyser settings and its characteristic frequency response (flatness).

#### 4. Theoretical model and numerical simulations

The theoretical model proposed in the paper is based on the delay differential equation approximation and aims to predict the basic operating behavior of a GaAs-based monolithic two-section quantum-dot laser. The particular goal was to highlight the underlying physical mechanisms that govern the dual-wavelength mode-locked operation. The equations have been previously reported in the literature, but it is the first time to our knowledge that they are combined in a single model that takes into account both GS and ES emission with individual delay equation for each state.

The theoretical analysis is focused on the dual-wavelength mode-locked operation observed in the experiments as well as the clarification of the underlying physical mechanisms which control this operating regime. Furthermore, the different operation regimes are reproduced by the model and briefly reported in this paper. The numerical model is based on the delay differential equation approximation [11] to describe the cavity effects enhanced with multipopulation rate equations to account for the dynamics of quantum dot material [12]. An active (gain) and a passive (absorber) sections as well as a bandwidth limiting element are included. Moreover, a ring-cavity geometry with unidirectional operation is assumed. The evolution of the fields in the gain and absorbing sections follows the delay equation [11]:

$$\frac{\partial A_n(t)}{\partial t} = \frac{\kappa}{\tau_p} e^{(1+i\alpha_g)L_g g(t-\tau_d)/2 + (1+i\alpha_q)L_q q(t-\tau_d)/2} A_n(t-\tau_d) - \frac{1}{\tau_p} A_n(t) \quad (1)$$

where  $A_n(t)$  is the slow envelope of the field for state  $n$  (GS, ES).  $g$  and  $q$  are the gain and absorbing coefficients for the active and passive section respectively,  $\alpha_g$  and  $\alpha_q$  are the corresponding linewidth enhancement factors, and  $L_g$  and  $L_q$ , are the corresponding round trip propagation lengths in the gain and absorbing section, respectively. Moreover,  $\tau_d$  is the round-trip delay time of the cavity,  $\kappa$  is the round-trip attenuation factor and  $\tau_p^{-1}$  is the bandwidth of the bandwidth limiting element.

The quantum dot model describes the dot energy distribution with a multi-population rate equation set, accounting only for the electron dynamics (excitonic representation) [12]. The model includes three energy states, the wetting layer (WL) which is the common carrier reservoir, the excited state which captures the electrons from WL and the ground state. The carrier density rate equations for each state of the gain section are:

$$\frac{\partial n_{WL}(t)}{\partial t} = \frac{I}{eV} + \sum_j \frac{n_{ES}^j}{\tau_{ES-WL}} - \frac{n_{WL}}{\tau_{WL-ES}^{mean}} - \frac{n_{WL}}{\tau_{spon,WL}} \quad (2)$$

$$\frac{\partial n_{ES}^j(t)}{\partial t} = \frac{G^j n_{WL}}{\tau_{WL-ES}^j} + \frac{n_{GS}^j}{\tau_{GS-ES}^j} - \frac{n_{ES}^j}{\tau_{ES-WL}} - \frac{n_{ES}^j}{\tau_{ES-GS}^j} - \frac{n_{ES}^j}{\tau_{spon,ES}} - \nu_g g_{ES}^j |A_{ES}(t)|^2 \quad (3)$$

$$\frac{\partial n_{GS}^j(t)}{\partial t} = \frac{n_{ES}^j}{\tau_{ES-GS}^j} - \frac{n_{GS}^j}{\tau_{GS-ES}^j} - \frac{n_{GS}^j}{\tau_{spon,GS}} - \nu_g g_{GS}^j |A_{GS}(t)|^2 \quad (4)$$

where  $n_{WL}(t)$  is the carrier density of the wetting layer, and  $n_{ES}^j$ ,  $n_{GS}^j$  are the carrier density of the  $j$ -th dot group for the excited and ground state, respectively;  $g_{ES}^j$  and  $g_{GS}^j$  are the corresponding gain coefficients.  $\tau_{ES-GS}^j$  and  $\tau_{GS-ES}^j$  are the the  $j$ -th dot group characteristic times for the electron transition from excite to ground state and from ground to excited state, respectively;  $\tau_{WL-ES}^{mean}$ ,  $\tau_{WL-ES}^j$ ,  $\tau_{ES-WL}$  are the carrier capture and escape time, respectively, for the transition between the wetting layer and the dots [13]. The spontaneous emission rates are calculated through the carrier lifetime for each state:  $\tau_{spon,WL}$ ,  $\tau_{spon,ES}$  and  $\tau_{spon,GS}$ . The transition times from state  $n_1$  to  $n_2$  depend on the state occupation probability  $P_n^j$ , and they are calculated by  $\tau_{n_1-n_2}^j = \tau_{n_1-n_2}^0 / (1 - P_{n_2}^j)$  [13]. Finally,  $V$  is the active region volume and  $I$  is the injected current. Similar expressions to (2) – (4) stand for the absorbing section as well, enhanced by additional sweep-out terms (as in [14]) in order to take into account the dependence of the absorber dynamics on the applied negative voltage due to thermionic and tunneling carrier escape mechanisms.

The gain (and similarly the absorption) coefficient for the state  $n$  and for the dot group  $j$  at the frequency  $\omega$  is given by [12]:

$$g_n^j(t, \omega) = F_g \frac{D_n}{\hbar \omega_n^j} (2P_n^j - 1) G^j(\omega_n^j) L_n^j(\omega) \quad (5)$$

where the coefficient  $F_g$  includes the volume quantum dot density, the transition matrix element and constants.  $D_n$  is the degeneracy of the state,  $\omega_n^j$  is the central frequency if the  $j$ -th dot group for state  $n$ . The term  $G^j(\omega_n^j)$  accounts for inhomogeneous broadening of the gain due to the dot size fluctuation and it is described by a Gaussian distribution [13]; the homogeneous broadening of the gain is assumed to be a Lorentzian distribution and it is

described by  $L_n^j(\omega)$  [12].  $P_n^j$  is the state occupation probability given by:  $P_n^j = n_n^j / (2D_n N_D^{vol} G^j(\omega_n^j))$  [12] where  $N_D^{vol}$  is the volume dot density. The total gain/absorption coefficient in (1) is given by the summation over all quantum dot groups and states. The values of the most significant parameters are given below. The spontaneous recombination times are  $\tau_{spont,WL} = 5$  ns,  $\tau_{spont,ES} = 500$  ps and  $\tau_{spont,GS} = 2$  ns; the transition times are  $\tau_{ES-GS}^0 = 8$  ps,  $\tau_{GS-ES}^0 = 18$  ps,  $\tau_{WL-ES}^0 = 2$  ps,  $\tau_{ES-WL}^0 = 10$  ps. The full width at half maximum of the inhomogeneous broadening is 50 meV and the corresponding width of the homogeneous broadening is 16.5 meV. The linewidth enhancement factor for the gain and absorber are  $\alpha_g = 2$  and  $\alpha_q = 2$ . The degeneracy of the states are  $D_{ES} = 4$  and  $D_{GS} = 2$ . The interband transition matrix element is  $2.7 \times 10^{-49}$  eV Kg. Finally the quantum dots volume density is  $N_D^{vol} = 3.7 \times 10^{22}$  m<sup>-3</sup>.

Since the main purpose of the numerical evaluation is not to obtain a complete mapping of the specific laser configuration but to focus on the dual-wavelength mode-locked operation, some of the parameters are fitted to match the simultaneous GS-ES operation regime.

At the region near the threshold of the GS ( $I_G = 1.1I_{th} - 2.0I_{th}$ ) stable mode-locked operation is observed, strongly dependent on the absorber voltage value. At low values of reverse bias voltages in the absorber section (i.e.  $V < 6$  V) continuous wave (CW) operation, including regions with intensity fluctuations, at the GS is observed (slow absorber). However, at higher bias values (i.e.  $V > 6$  V) stable GS mode-locking (GS-ML) is revealed due to the fast absorption recovery time, assisted by the sweep-out effect. A typical GS-ML time trace calculated at  $I = 1.2I_{th}$  and  $V = 10$  V with a pulse width close to 3 ps is depicted in Fig. 4. A slight asymmetry in the pulse is attributed to the fast absorption saturation responsible for pulse leading edge shaping. Additionally, the calculated optical spectrum has a free spectral range (FSR) corresponding to a repetition rate frequency in the order of 20 GHz. Furthermore, for current values higher than  $2.0I_{th}$  and up to  $2.7I_{th}$ , GS-CW wave or GS-ML is observed for different values of the absorber voltage.

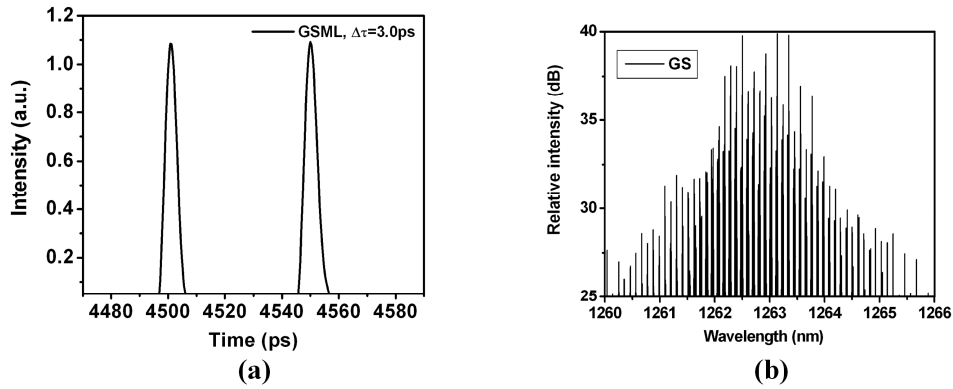


Fig. 4. (a) Time trace for pulse generated from GS mode-locking and (b) the corresponding optical spectrum.

According to our calculations, at low gain currents ES is almost unpopulated. However, at current values of  $I_G = 2.7I_{th} - 2.8I_{th}$  GS emission saturates, ES carrier population increases and gradually ES lasing is observed. The onset of ES emission is accompanied with a stable ES-ML for reverse bias voltages larger than 6 V due to the respective decrease of the absorber recovery time, as it has already been mentioned above. In the range of gain current between  $2.8I_{th}$  and  $3.4I_{th}$ , ES ML coexists with unstable GS-CW operation.

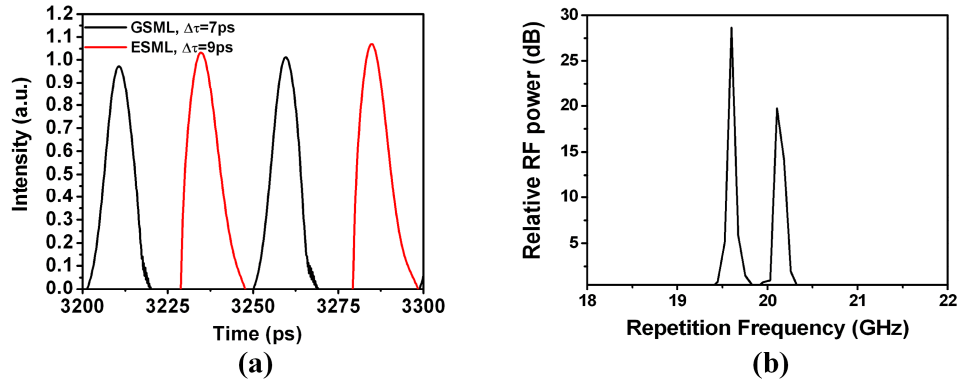


Fig. 5. (a) Time traces for pulses generated from simultaneous GS-ES mode-locking and (b) the corresponding simulated RF spectrum.

In agreement with the experiments, a region with stable dual-wavelength mode-locking occurs at a relatively narrow current range ( $I_G = 3.4I_{th} - 3.7I_{th}$ ) and for bias voltages higher than 7 V. The calculated pulse time traces of this regime are shown in Fig. 5. The GS and ES pulses are shifted to each other in accordance with out-of-phase dynamics between the two states. This effect can be attributed to the asymmetric power exchange during capture/escape carrier transitions which result to nonlinear amplitude-phase coupling [15]. The generated pulses from the stable dual-wavelength mode-locked operation are broadened [Fig. 5(a)] for both GS ( $\Delta\tau = 6.5$  ps) and ES pulse ( $\Delta\tau = 9$  ps) compared to the GS-ML, due to the high gain current value needed for the appearance of lasing from the ES. The relatively narrow regime of dual-wavelength mode-locked operation can be attributed to the dynamics between the two competitive states due to the carrier intraband capture/escape process between them, giving rise to instabilities. At gain currents beyond  $3.8I_{th}$ , ES-ML is observed while at even higher current values (i.e.  $I > 4.2I_{th}$ ) ES-CW is observed. In both cases emission from GS is suppressed.

The theoretical computations are in good qualitative agreement with the experimental results. The main trends of the experimental mapping are clearly reproduced by the model. Some differences exist in transitions between distinct operating regions where generally unstable operation occurs. In these regions, the model shows quasi-CW operation with fast fluctuations of the output power, condition that cannot be experimentally observed.

## 5. Conclusion

In this paper we report the first experimental and theoretical investigation of a dual-wavelength passive mode-locking regime where pulses are generated from both ES ( $\lambda = 1180\text{nm}$ ) and GS ( $\lambda = 1263\text{nm}$ ), in a two-section GaAs-based QD laser. The spectral separation (83nm) is the widest ever observed in a dual-wavelength mode-locked non-vibronic laser. Additionally, numerical simulations are presented by means of a theoretical model based on the delay differential equation approximation, which reproduce the dual-wavelength mode-locking regime. The exploitation of this mode-locked regime could enable a range of applications extending from time-domain spectroscopy, through to optical interconnects, wavelength-division multiplexing and ultrafast optical processing.

## Acknowledgements

The work was funded within the Seventh Framework Program “FAST-DOT”, through Grant No. 224338. M. A Cataluna acknowledges also financial support through a Royal Academy of Engineering/EPSC Research Fellowship.